

# Thermal boundary resistance and thermal conductivity of multiwalled carbon nanotubes

Ravi Prasher\*

Intel Corporation, 5000 W. Chandler Boulevard, Chandler, Arizona 85226-3699, USA

(Received 15 March 2007; published 25 February 2008)

Thermal boundary resistance (Kapitza resistance) and thermal conductivity of multiwalled carbon nanotubes (MWCNTs) are calculated assuming the properties of graphite in the temperature range of 10–100 K. By including the thermal boundary resistance between the MWCNT and the measuring device, calculated thermal conductivity of MWCNT is in very good agreement with the experimental data of Kim *et al.* [Phys. Rev. Lett. **87**, 215502 (2001)], showing that the thermal behavior of MWCNTs is similar to graphite. Thermal conductivity of MWCNT as measured by Kim *et al.* is smaller than the thermal conductivity of graphite fibers and pyrolytic graphite at low temperatures due to thermal boundary resistance. The intrinsic mean free path of phonons in MWCNTs in the temperature range of 10–100 K is found to be similar to the mean free path in graphite fibers. Finally, it is shown that the thermal boundary resistance could be one of the main reasons that the thermal conductivity of MWCNT bundles as measured by Kim *et al.* is lower than the thermal conductivity of a single MWCNT.

DOI: 10.1103/PhysRevB.77.075424

PACS number(s): 65.80.+n, 66.70.-f, 63.22.-m

## I. INTRODUCTION

Thermal properties of carbon nanotubes are of fundamental interest.<sup>1–12</sup> They also play a critical role in controlling the performance and stability of nanotube devices.<sup>3,4</sup> Some other applications of carbon nanotubes are in composites, thermal interface materials, and nanofluids.<sup>7–12</sup> Kim *et al.*<sup>1</sup> and Fujii *et al.*<sup>2</sup> reported very high experimentally measured thermal conductivity of multiwalled carbon nanotubes (MWCNTs) at room temperature. On the theoretical front, Mingo and Broido<sup>5</sup> performed calculations of ballistic thermal conduction in single walled carbon nanotubes (SWCNTs) and MWCNTs assuming phonon dispersion of graphite. They found that the thermal conductance of MWCNT measured by Kim *et al.*<sup>1</sup> was 2.5 times smaller than the ballistic thermal conductance at low temperatures. Based on their theoretical study, it seems that MWCNTs are different from graphite in their thermal behavior at low temperatures. The first objective of this paper is to carefully analyze the data by Kim *et al.*<sup>1</sup> to understand if MWCNTs are really different than graphite at low temperatures.

The second objective of this paper is to calculate the thermal boundary resistance (Kapitza resistance) between MWCNTs and bulk substrates. Thermal boundary resistance is important in various applications and metrologies.<sup>1–12</sup> For example, in the measurement of thermal conductivity of MWCNTs by Kim *et al.*<sup>1</sup> and Fujii *et al.*,<sup>2</sup> MWCNTs were in contact along the length with a bulk substrate (horizontal contact). Therefore, the effective thermal conductivity reported in these two studies includes the thermal boundary resistance ( $R_c$ ). It is important to separate  $R_c$  and thermal conduction in the bulk of MWCNTs to clearly understand the thermal transport mechanisms in MWCNTs. Mingo and Broido<sup>5</sup> neglected  $R_c$  in their calculations while comparing their calculations with the experimental data. As-grown vertically oriented MWCNTs on a substrate<sup>7–9</sup> or MWCNTs embedded in an elastic medium to form composites<sup>10,11</sup> have been proposed to be used as thermal interface materials. Knowledge of  $R_c$  is also very important in these applications.

Therefore,  $R_c$  is calculated for both vertical and horizontal contacts.

Kim *et al.*<sup>1</sup> also measured the thermal conductivity of MWCNT bundles. Thermal conductivity of bundles in their study was significantly smaller than the thermal conductivity of a single MWCNT. Their data also showed that thermal conductivity of larger bundles was smaller than the thermal conductivity of smaller bundles. Thermal conductivity of graphite fiber bundles has shown no such effects.<sup>13</sup> The third objective of this paper is to understand the reasons behind smaller conductivity of bundles as compared to a single MWCNT.

## II. THERMAL CONDUCTIVITY OF MULTIWALLED CARBON NANOTUBES AND GRAPHITE

To clearly understand the differences between MWCNTs and graphite, thermal conductivity of pyrolytic graphite and graphite fibers<sup>13–18</sup> grown at very high temperatures is compared with the thermal conductivity of MWCNTs from the measurements of Kim *et al.*<sup>1</sup> and Fujii *et al.*<sup>2</sup> in Fig. 1. Kim *et al.*<sup>1</sup> reported an uncertainty of the order of 2 nm in their MWCNT diameter. Figure 1 shows their data by assuming 14 nm diameter (reported diameter) and 16 nm diameter.

Figure 1 shows that the thermal conductivity of graphite from various sources match very well at low temperatures. At low temperatures, mean free path (mfp) of phonons in graphite is typically dominated by crystallite and grain boundaries, leading to a constant mfp.<sup>18,19</sup> Figure 1 shows that at low temperatures (<100 K), thermal conductivity of pyrolytic graphite and vapor grown graphite fibers are approximately the same, indicating that their mfp is the same. Heremans and Beetz<sup>18</sup> found that mfp of graphite fibers for temperatures <100 K was  $\sim 2.9 \mu\text{m}$ .

Figure 1 shows that at low temperatures ( $T < 100$  K), thermal conductivity of MWCNTs measured by both Kim *et al.*<sup>1</sup> and Fujii *et al.*<sup>2</sup> is much smaller than the thermal conductivity of graphite. This suggests that MWCNTs are different than graphite in their thermal behavior. Some potential

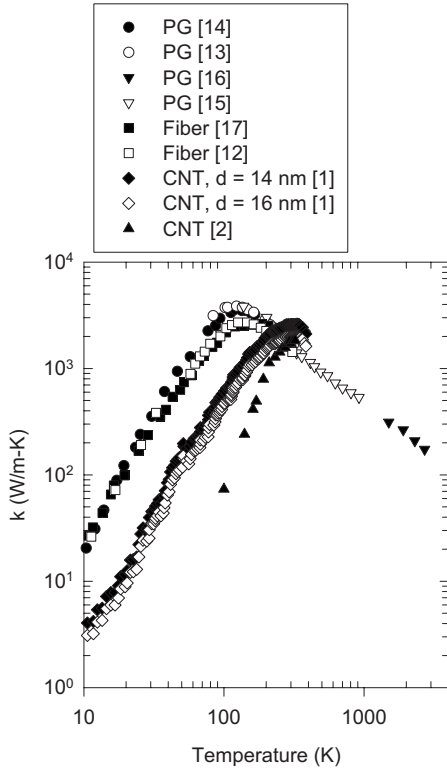


FIG. 1. Comparison between the thermal conductivity of MWCNTs and graphite. Kim *et al.* (Ref. 1) reported an error of 2 nm in MWCNT diameter with a nominal diameter of 14 nm. Thermal conductivity from their data is shown by assuming diameters of 14 nm and 16 nm. Larger diameter gives smaller thermal conductivity, making it closer to the graphite thermal conductivity at higher temperatures (after the maxima).

reasons for this behavior could be (1) ballistic transport of phonons in the MWCNTs owing to the small length of MWCNTs investigated in the experiments,<sup>1,2</sup> and (2) smaller intrinsic mfp in MWCNTs as compared to graphite at low temperatures. Both these effects will result in the decrease in the thermal conductivity of MWCNTs at low temperatures.<sup>20</sup>

It is shown in this paper that thermal conductivity of MWCNTs is lower than the thermal conductivity of graphite in the low-temperature regime due to the presence of thermal boundary resistance between the MWCNTs and the measuring device and due to the semiballistic transport in MWCNTs. Both these effects reduce the effective mfp at low temperatures. This leads to reduced thermal conductivity at low temperatures. This paper is focused on the low-temperature regime (<100 K) to clearly identify the reasons behind smaller thermal conductivity of MWCNTs in comparison with the thermal conductivity of graphite.

### III. PHONON DISPERSION AND SPECIFIC HEAT OF MULTIWALLED CARBON NANOTUBES AND GRAPHITE

The phonon dispersion relation is discussed in this section to show under which conditions phonon dispersion in bulk graphite can be used for describing phonon transport in

TABLE I. Physical properties and different parameters of graphite used in calculations (Ref. 23).

$d$	0.335 nm
$v_L$	$2.01 \times 10^4$ m/s
$v_T$	$1.23 \times 10^4$ m/s
Debye velocity in basal plane ( $v_D$ )	$2/v_D^2 = 1/v_L^2 + 1/v_T^2$ $v_D = 1.48 \times 10^4$ m/s
$c_{44}$	2.26 GPa
$c_{33}$	36 GPa
$\delta$	$6.11 \times 10^{-7}$ m <sup>2</sup> /s
$q_{a,max}$	$1.55 \times 10^{10}$ m <sup>-1</sup>
$q_{z,max}$	$1.88 \times 10^{10}$ m <sup>-1</sup>
$\rho$	2260 kg/m <sup>3</sup>
$\nu$	0.012

MWCNTs. Phonon dispersion in graphite is discussed first. In bulk three-dimensional (3D) isotropic solids, there are three modes of vibrations: one longitudinal and two transverse. Bulk graphite is not isotropic because it has different properties in the basal plane and in the  $c$ -axis direction; however, it still has three modes: one longitudinal, one transverse, and one out-of-plane mode. Two-dimensional (2D) graphene, which forms the adjacent layers in graphite, also has three modes: one longitudinal, one transverse, and one out-of-plane flexural mode.

Since the focus of the paper is on the low temperature regime ( $T < 100$  K), semicontinuum dispersion relation by Kumatsu<sup>21</sup> is used. Kumatsu's dispersion relation has been consistently used by Heremans and Beetz,<sup>18</sup> Kelly,<sup>22,23</sup> and Reynolds<sup>24</sup> in calculating the thermal conductivity and specific heat of graphite. Kumatsu's dispersion relation gives accurate results for the specific heat of graphite up to 100 K,<sup>21,24</sup> which is the temperature range of interest in this paper. The dispersion relation for three polarizations of phonons (longitudinal, transverse, and out of plane) is given as<sup>21,22</sup>

$$\omega_1^2 = v_L^2 q_a^2 + \frac{4c_{44}}{d^2 \rho} \sin^2\left(\frac{dq_z}{2}\right), \quad (1a)$$

$$\omega_2^2 = v_T^2 q_a^2 + \frac{4c_{44}}{d^2 \rho} \sin^2\left(\frac{dq_z}{2}\right), \quad (1b)$$

$$\omega_3^2 = \delta^2 q_a^4 + \frac{c_{44}}{\rho} q_a^2 + 4 \frac{c_{33}}{\rho d^2} \sin^2\left(\frac{dq_z}{2}\right), \quad (1c)$$

where  $\omega$  is the frequency,  $v_L$  the longitudinal velocity,  $v_T$  the transverse velocity,  $d$  the interlayer separation distance,  $\rho$  the mass density of graphite, and  $q$  the wave vector.  $\delta$ ,  $c_{33}$ , and  $c_{44}$  are elastic constants. Subscript  $a$  denotes the basal plane in this paper. The  $c$  axis is given by the  $z$  direction. The terms involving  $c_{33}$  and  $c_{44}$  in Eqs. (1a)–(1c) reflect the coupling between adjacent graphene layers due to the van der Waals force.<sup>22</sup> Different parameters needed in Eq. (1) are given in Table I. Experimental values of  $c_{33}$  from different studies do not vary much<sup>22,25</sup> but values of  $c_{44}$  vary in a large range.<sup>22,25</sup>

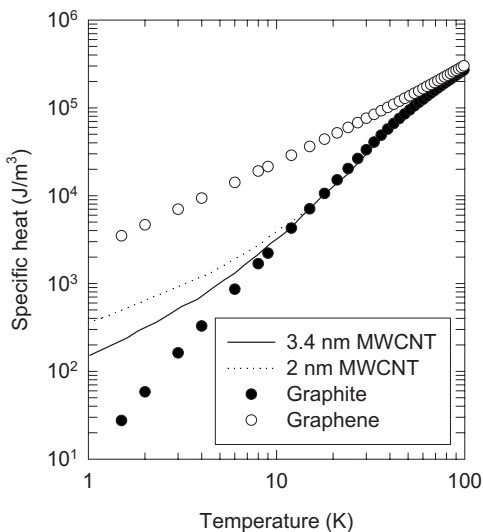


FIG. 2. Theoretical specific heat of graphite, graphene, and MWCNTs assuming the properties of graphite. Curves for 3.4 and 2 nm MWCNTs taken from Ref. 43. The figure clearly shows that deviation from the bulk behavior due to phonon confinement takes place at very low temperatures. For 14 nm MWCNT used by Kim *et al.* (Ref. 1), significant deviation will take place at  $T \sim 2.5$  K (see text for details).

The value of  $c_{44}$  recommended by Kelly<sup>23</sup> is taken here for graphite.

Note that  $q_a^2 = q_x^2 + q_y^2$ , where  $q_x$  and  $q_y$  are the wave vectors in  $x$  and  $y$  directions, respectively. The Brillouin zone in graphite is disk shaped<sup>19,22</sup> due to the difference in the lattice constants in the  $a$  plane and  $c$  direction. Equations (1a)–(1c) give different phonon velocities in the basal plane and the  $c$  direction, i.e., phonon dispersion is anisotropic. By putting  $c_{33} = 0$  and  $c_{44} = 0$  in Eqs. (1a)–(1c), the dispersion relation for the 2D graphene sheet is obtained.<sup>26</sup>

Specific heat (heat capacity/unit volume) of a material at low temperature provides very valuable information regarding the phonon dispersion and its impact on thermal properties. Therefore, specific heat of graphite and graphene are calculated using Eqs. (1a)–(1c). Specific heat calculations are also shown to understand the differences in the phonon dispersion of graphite and MWCNTs. The specific heat ( $C$ ) is given by

$$C = \frac{1}{(2\pi)^3} \sum_3 \int_q \hbar \omega \frac{df}{dT} dq$$

$$= \frac{1}{(2\pi)^2} \sum_3 \int_0^{q_{a, \max}} \int_0^{q_{z, \max}} \hbar \omega \frac{df}{dT} q_a dq_a dq_z, \quad (2)$$

where  $q_{a, \max}$  is the maximum value of the basal plane wave vector,  $q_{z, \max}$  the maximum value of the  $c$ -axis wave vector,  $\hbar$  the reduced Planck constant, and  $f$  the Planck function. Values of  $q_{a, \max}$  and  $q_{z, \max}$  are given in Table I. Summation in Eq. (2) indicates summation for three polarizations of phonons. Figure 2 shows the specific heat of graphite and graphene. Figure 2 shows that for  $T > 50$  K, the specific heat of graphite merges with the specific heat of 2D graphene.

The reason for this behavior is that  $c$ -axis phonons in graphite have low frequencies due to weak interactions between the graphene layers. Therefore, at higher temperatures ( $T > 50$  K), the interlayer phonon modes are fully occupied.<sup>1,27</sup>

The question that remains to be answered is whether the phonon dispersion of bulk graphite can be used for describing the specific heat and the thermal conductivity of MWCNTs because MWCNTs are concentric cylinders of graphene sheets.<sup>27</sup> Both nanowires and nanotubes can have different phonon dispersions than their bulk counterparts due to two reasons:<sup>27–35</sup> (1) confinement of phonons because of waveguiding effects,<sup>30–34</sup> and (2) elastic modulus, which effectively determines the phonon velocity, is different in the nanostructures than their bulk counterparts.<sup>27–29</sup>

Phonon confinement (or waveguiding) effects are discussed first. Phonon confinement gives rise to multiple bands.<sup>30–32</sup> These bands are obtained by applying stress-free boundary conditions at the inner and outer surfaces of a nanotube or at the outer surface of a nanowire<sup>32</sup> and then solving the 3D wave equation. The four lowest lying modes ( $\omega = 0$  at  $q = 0$ ) are one longitudinal, one torsional, and two flexural. SWCNTs are a special case where the modes are obtained by solving the 2D wave equation because SWCNTs are assumed to be single atomic layers of graphite or graphene (also called 2D graphite) rolled to form tubes.<sup>36</sup> Dresselhaus and Eklund<sup>36</sup> have extensively discussed the phonon dispersion of SWCNTs. SWCNTs also have four lowest lying modes; however, there has been a bit of confusion regarding the four lowest lying modes in SWCNTs. Dresselhaus and Eklund<sup>36</sup> showed by using zone-folding formulations that the four lowest modes in SWCNTs are one longitudinal, two tangential, and one twist mode. All these modes follow linear phonon dispersion, i.e.,  $\omega \propto q$ . Later, other groups<sup>33–35</sup> showed that although there are four lowest lying modes in SWCNTs, however, they are just like any other nanowire or nanotube, i.e., there are one longitudinal, one torsional, and two flexural modes. Unlike the linear dispersion of tangential modes obtained by the analysis of Dresselhaus and Eklund,<sup>36</sup> the flexural modes follow a quadratic dispersion, i.e.,  $\omega \propto q^2$ . The main reason for the discrepancy between the analysis of Dresselhaus and Eklund<sup>36</sup> and that of other groups<sup>33–35</sup> is that zone-folding formulations are strictly valid for scalar waves, whereas phonons are vector waves. Mahan and Jeon have<sup>34</sup> discussed this extensively.

All the modes and bands due to phonon confinement in nanowires and nanotubes can be obtained by rigorously solving the wave equation using standard techniques;<sup>32</sup> however, it is very tedious. Therefore, in the next paragraphs, the conditions under which phonon dispersion for bulk solid can be applied to nanowires or nanotubes are discussed. This discussion assumes that the intertube coupling in MWCNTs is the same as the interlayer coupling in graphite. Validity of this assumption is discussed later.

Different regimes of wave transport can be described in a tube based on the values of  $qr_2$  and  $q(r_2 - r_1)$ , where  $q$  is the wave vector and  $r_2$  and  $r_1$  are the outer and inner radii of the tube, respectively. Waves in a tube can be described using the bulk 3D waves if<sup>32</sup>  $qr_2 \gg 1$  and  $q(r_2 - r_1) \gg 1$ . For  $qr_2 \gg 1$  but  $q(r_2 - r_1) \ll 1$ , waves in a tube behave as 2D waves in

thin sheets.<sup>32</sup> For  $qr_2 \ll 1$ , the waves are purely one dimensional (1D) and the tube behaves as a 1D bar.<sup>32</sup> Therefore, phonon confinement effects are very important for both thermal transport and specific heat when dominant wavelength of phonons becomes comparable to the size of the nanotube. The dominant frequency or wave vector can be estimated by finding the frequency where the maximum of the frequency-dependent specific heat ( $C_\omega$ ) occurs with respect to the frequency.<sup>37</sup> Note that some authors have also used the maximum of the internal energy to define the dominant frequency.<sup>38,39</sup> The dominant frequency of graphite can be estimated as  $\hbar\omega_d = \hbar v q_d \approx 2.6k_b T$  using density of states (DOS) of graphite,<sup>22</sup> where  $k_b$  is the Boltzmann constant,  $v$  the speed of phonons,  $q_d$  the dominant wave vector, and  $\omega_d$  the dominant frequency. The DOS of graphite is more complicated than the DOS of isotropic solids. While calculating  $\omega_d$ , DOS applicable at large temperatures is assumed (assuming 2D behavior). At very low temperatures, graphite behaves like quasi-3D solids (specific heat of graphite varies as  $T^3$  for very small  $T$ ). For perfectly 3D solid,<sup>37</sup>  $\hbar\omega_d = \hbar v q_d \approx 3.83k_b T$ . Therefore, estimation of  $\omega_d$  or  $q_d$  is more conservative.

Note that these discussions are applicable to both isotropic and anisotropic solids. For most solids, the dominant phonon wavelength is very small at room temperature; however, it can be a few hundred nanometers at very low temperatures. For example, to observe effects of phonon confinement on thermal transport, Schwab *et al.*<sup>40</sup> conducted their experiments on a silicon nitride catenoidal nanomembrane at very low temperatures. They observed that the thermal conductance reduced to the universal quantum conductance<sup>30</sup> of a 1D conductor for  $T < 0.8$  K. Prasher<sup>41</sup> showed recently that after 0.8 K, data by Schwab *et al.*<sup>40</sup> could be very well described using 3D phonon dispersion.

Assuming Debye velocity in the basal plane (Table I),  $q_d = 0.229 \text{ nm}^{-1}$  at  $T = 10$  K for graphite. The outer diameter of MWCNT used by Kim *et al.*<sup>1</sup> was 14 nm, whereas the inner diameter was very small,<sup>42</sup> i.e.,  $q(r_2 - r_1) \approx qr_2$ . At 10 K (lowest experimental temperature),  $q_d r_2 \approx 1.6$ , i.e.,  $q_d r_2 > 1$  in the entire experimental temperature range. Therefore, it is expected that graphite phonon dispersion should be applicable in the temperature range considered by Kim *et al.*<sup>1</sup>

A more rigorous proof of whether bulk graphite dispersion is applicable to MWCNTs is the comparison of specific heat of MWCNTs calculated by considering all the phonon bands and modes obtained from solving the wave equation with stress-free boundary conditions with the specific heat calculated by assuming bulk graphite dispersion. Specific heat due to all the modes is given by

$$C = \frac{1}{A} \sum_s \frac{1}{\pi} \int_{\omega_s}^{\omega_{\max}} \frac{df}{dT} \hbar \omega d q_l = \frac{1}{A} \sum_s \frac{1}{\pi} \int_{\omega_s}^{\omega_{\max}} \frac{df}{dT} \hbar \omega \left( \frac{d q_l}{d \omega} \right) d \omega, \quad (3)$$

where  $s$  signifies the mode numbers,  $q_l$  is the phonon wave vector in the axial direction of the nanotube (nanowire), and  $A$  is the cross sectional area of the nanotube (nanowire). Note that Eq. (3) also includes the four fundamental modes ( $\omega = 0$  at  $q_l = 0$ ). The difference between successive phonon

bands (modes), i.e.,  $\Delta\omega$ , goes as<sup>32</sup>  $\Delta\omega \propto 1/r$ . Therefore, for larger radius,  $\Delta\omega \rightarrow 0$  due to which the summation in Eq. (3) can be converted into an integral which results in the 3D formulation of specific heat.

Popov<sup>43</sup> calculated the specific heat of MWCNTs. Figure 2 shows the comparison between the theoretical calculations of Popov<sup>43</sup> for two MWCNTs of different diameters. Figure 2 shows that the specific heat of 3.4 nm MWCNT is the same as the specific heat of graphite for  $T > 10$  K and the specific heat of 2 nm MWCNT is same as the specific heat of graphite for  $T > 18$  K. This corresponds to  $q_d r \approx 0.4$ , in all cases assuming Debye velocity (Table I) in the basal plane. Popov calculated the specific heat for other diameters as well. In all the cases, the transition to the graphite specific heat takes place for  $q_d r \approx 0.4$ . This shows that even for  $q_d r < 1$ , the specific heat of MWCNTs can be described using the bulk phonon dispersion of graphite. Since  $q_d$  is proportional to  $T$ , the transition temperature from bulk behavior to 1D behavior is given by  $T_{1D} \propto 1/r$ , assuming that  $q_d r \approx 0.4$ . Based on this,  $T_{1D}$  for the MWCNT used by Kim *et al.*<sup>1</sup> is  $\sim 2.5$  K ( $r = 7$  nm). This means that below 2.5 K, majority of the contribution to the specific heat will come from the four lowest lying modes (only modes available in purely 1D bar as mentioned earlier), whereas above this temperature, contribution of the higher modes becomes important as higher modes get excited, making the specific heat of MWCNTs closer to the specific heat of bulk solid (graphite). Therefore, phonon confinement effects are not important in analyzing the data by Kim *et al.*<sup>1</sup> as they collected data for  $T > 10$  K.

In the previous discussions, it was assumed that intertube coupling in MWCNTs is the same as the interlayer coupling in graphite; however, this assumption is questionable considering that graphene layers in graphite are planar, whereas in MWCNTs, they are cylindrical. Due to the different diameters of adjacent cylinders of carbon atoms in the MWCNTs, the structural arrangement of the adjacent carbon honeycomb cylinders is not strongly correlated.<sup>27</sup> Since nanotubes are composed of nearly coaxial cylindrical layers, each possibly with different helicities, the adjacent layers are generally noncommensurate (e.g., zigzag and/or armchair),<sup>25,27,44</sup> i.e., stacking cannot be classified as AA or AB as in graphite. The consequence of this interplanar stacking disorder is a decreased coupling between the layers relative to coupling in graphite. Due to these reasons, the stacking arrangements of nanotubes are expected to be similar to turbostratic graphite.<sup>27</sup> Turbostratic graphite means graphite whose adjacent basal planes are randomly rotated with respect to one another.<sup>45</sup> The decreased coupling between adjacent layers in MWCNTs should result in smaller values of interlayer elastic constants  $c_{33}$  and  $c_{44}$  as they are dependent on the strength of interlayer coupling due to van der Waals forces.<sup>22</sup> The extreme case of weak coupling is that there is no coupling between the tubes, i.e., the individual tubes behave as separate sheets of graphene. However, in various studies on the mechanical properties of MWCNTs, interlayer coupling was assumed to be the same as that in graphite.<sup>25,46</sup> There has been one direct measurement of the elastic constant  $c_{33}$  of MWCNT by Palaci *et al.*<sup>47</sup> Palaci *et al.*<sup>47</sup> concluded that  $c_{33}$  of large diameter ( $> 10$  nm) MWCNTs was almost the same as  $c_{33}$  of graphite. The value of  $c_{33}$  obtained by them was

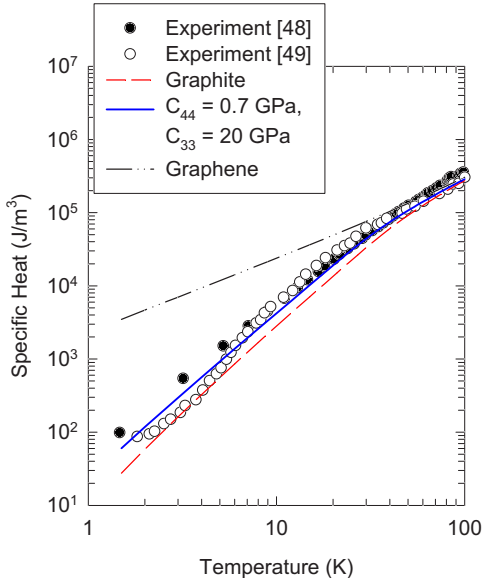


FIG. 3. (Color online) Calculated specific heat of MWCNT in comparison with experimental data.  $c_{44}=0.7$  GPa and  $c_{33}=20$  GPa reflect the reduced coupling between the graphene layers in MWCNTs (see text for details).

$30 \pm 10$  GPa, which is comparable to  $c_{33}$  of graphite which is 36 GPa (Table I).

Whether interlayer coupling in MWCNTs is vastly different from that in graphite can be assessed by comparing the specific heat of MWCNTs at low temperatures with theoretical calculations based on assuming graphite dispersion. At high temperatures, specific heats of graphite and graphene are almost the same (Fig. 2). Only at low temperatures, the interlayer coupling is important for specific heat. Figure 3 shows the comparison between the calculated specific heat assuming the properties of graphite and the experimental data by Mizel *et al.*<sup>48</sup> and Masarapu *et al.*<sup>49</sup> Diameter of the MWCNTs used by Mizel *et al.*<sup>48</sup> was 10–20 nm and that by Masarapu *et al.*<sup>49</sup> was 25–30 nm. Therefore, phonon confinement effects are expected to be important only at very low temperatures, as discussed before. Figure 3 shows that although the calculated specific heat assuming the properties of graphite (Table I) is close to the experimental data, however, generally, it is lower than the experimental data. Figure 3 also shows that the experimental specific heat is closer to the calculated specific heat of graphite than it is to the specific heat of graphene. This shows that MWCNTs are coupled layers of graphene rather than completely uncoupled graphene sheets. At higher temperature, both the calculated specific heat of graphite and experimental specific heat are the same as the specific heat of graphene which is in line with the results shown in Fig. 2. As discussed earlier, the coupling between the adjacent graphene layers in MWCNTs is expected to be weaker than it is in graphite. The next set of calculations is performed by assuming different values of  $c_{33}$  and  $c_{44}$ . As noted previously, the data in the literature indicate a large variation in the value of  $c_{44}$ . A value of 0.7 GPa is assumed for  $c_{44}$  which is close to the  $c_{44}$  of turbostratic graphite.<sup>45</sup> The measured value of  $c_{33}$  of large diameter MWCNTs (>10 nm) by Palaci *et al.*<sup>47</sup> varied between 20

and 40 GPa. The lower limit is closer to the value of  $c_{33}$  for turbostratic graphite ( $\sim 27.7$  GPa) (Ref. 45) and the upper limit is close to the value of pyrolytic graphite (36 GPa). Figure 3 shows the calculated specific heat assuming  $c_{44}=0.7$  GPa and  $c_{33}=20$  GPa. Figure 3 also shows that the calculated specific heat is in good agreement with the experimental data.

Based on the discussions in this section, it is safe to say that MWCNTs behave as graphite although there is a possibility that the interlayer coupling in MWCNTs might be slightly weaker than it is in graphite. Therefore, thermal conductivity of MWCNTs has been calculated assuming both the recommended properties of graphite (Table I) and reduced values of  $c_{44}$  (0.7 GPa) and  $c_{33}$  (20 GPa). Unless stated otherwise, the results are presented assuming the properties given in Table I.

#### IV. MODELING OF THERMAL CONDUCTIVITY

The first set of calculations is performed assuming that the mfp of phonons in MWCNT is same as the mfp in graphite fibers, i.e., 2.9  $\mu\text{m}$ , and the transport is completely diffusive. The elements of the thermal conductivity tensor ( $k_{\alpha\beta}$ ) under relaxation time approximation is given by<sup>50</sup>

$$k_{\alpha\beta} = \sum_{m,q} \hbar \omega \frac{df}{dT} \eta(q) [v_{g,m}(q)]_{\alpha} \cdot [v_{g,m}(q)]_{\beta}, \quad (4)$$

where  $\eta$  is the mean scattering time,  $v_g$  is the group velocity,  $m$  denotes the phonon mode, and  $\alpha$  and  $\beta$  denote the direction ( $x$ ,  $y$ , or  $z$ ). For bulk solids, Eq. (4) can be converted into integral form. For isotropic bulk solids, Eq. (4) gives  $k = 1/3 \int C_{\omega} v_g l_{\omega} d\omega$ , where  $l_{\omega}$  is the mfp. Since phonon dispersion in the MWCNTs is assumed to be the same as the phonon dispersion in bulk graphite, Eq. (4) is converted into integral form. Since graphite is anisotropic, thermal conductivity in the basal plane or along the length of the MWCNT from Eq. (4) can be written as

$$k_a = \frac{1}{(2\pi)^3} \sum_3 \int \hbar \omega \frac{df}{dT} \eta v_{g,x}^2 dq, \quad (5)$$

where  $v_{g,x}$  is the group velocity in the  $x$  direction (direction of the heat flux). At low temperatures, mfp ( $l_a$ ) is a constant<sup>18,19,22</sup> which reduces Eq. (5) to

$$\begin{aligned} k_a &= \frac{l_a}{(2\pi)^3} \sum_3 \int_0^{2\pi} \int_0^{q_{a,\max}} \int_0^{q_{z,\max}} \hbar \omega \frac{df}{dT} v_{g,a} \\ &\quad \times \cos^2 \phi q_a dq_a dq_z d\phi \\ &= l_a \frac{\pi}{(2\pi)^2} \sum_3 \int_0^{q_{a,\max}} \int_0^{q_{z,\max}} \hbar \omega \frac{df}{dT} v_{g,a} q_a dq_a dq_z, \quad (6) \end{aligned}$$

where  $v_{g,a}$  is the group velocity in the  $a$  plane (basal plane) and  $\phi$  is the angle between  $v_{g,x}$  and  $v_{g,a}$ . Note that  $v_{g,a} = \partial\omega / \partial q_a$ .

Figure 4 shows that the predicted thermal conductivity assuming diffusive transport and mfp of graphite fibers is clearly much higher than the MWCNT data. The next set of

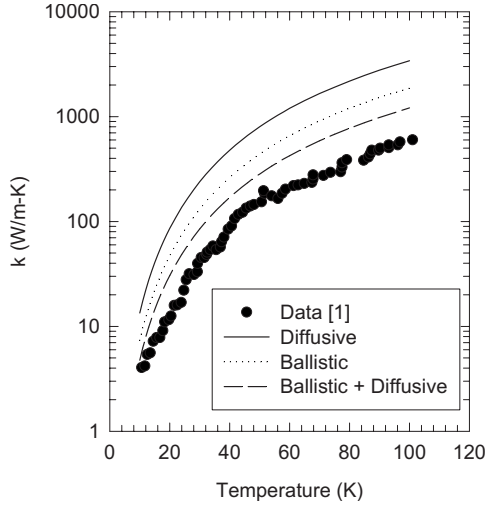


FIG. 4. Comparison between prediction and experimental data for MWCNT without including the contact resistance.

calculations is performed assuming that thermal transport is completely ballistic. The ballistic thermal conductance ( $G_B$ ) in the basal plane is given by

$$G_{B,a} = \frac{1}{2} \frac{1}{(2\pi)^3} \sum_3 \int_q \hbar \omega \frac{df}{dT} |v_{g,x}| dq. \quad (7)$$

Equation (7) can be written as

$$\begin{aligned} G_{B,a} &= \frac{1}{2} \frac{1}{(2\pi)^3} \sum_3 \int_0^{2\pi} \int_0^{q_{a,\max}} \int_0^{q_{z,\max}} \hbar \omega \frac{df}{dT} v_{g,a} \\ &\quad \times |\cos \phi| q_a dq_a dq_z d\phi \\ &= 2 \frac{1}{(2\pi)^3} \sum_3 \int_0^{q_{a,\max}} \int_0^{q_{z,\max}} \hbar \omega \frac{df}{dT} v_{g,a} q_a dq_a dq_z. \end{aligned} \quad (8)$$

Ballistic thermal conductivity can be defined by writing  $G_{B,a} = k_a/L$ , where  $L$  is the length of the MWCNT. Using  $G_{B,a} = k_a/L$ , Eqs. (6) and (8), effective mfp ( $l_B$ ) in the ballistic transport can be given as

$$l_{B,a} = (2/\pi)L. \quad (9)$$

Figure 4 shows that ballistic conductivity predictions are also much higher than the experimental data. The suspended length of the nanotube in the experiment<sup>1</sup> was  $\sim 2.5 \mu\text{m}$ . If it is assumed that the intrinsic mfp of MWCNT is the same as that of graphite fibers, i.e.,  $2.9 \mu\text{m}$ , then suspended length of the nanotube is comparable to the mfp. Therefore, the thermal transport is neither completely ballistic nor completely diffusive, i.e., it is semiballistic. In a series of papers,<sup>51</sup> the author has shown that in the semiballistic regime, adding the ballistic thermal resistance and diffusive thermal resistance is an excellent approximation. This approximation was in excellent agreement with the exact solution of the Boltzmann transport equation (BTE) for planar geometries, cylindrical geometries, and constrictions.<sup>51</sup> Similarly, Nikolic and Allen<sup>52</sup> and de Jong<sup>53</sup> showed that adding diffusive and bal-

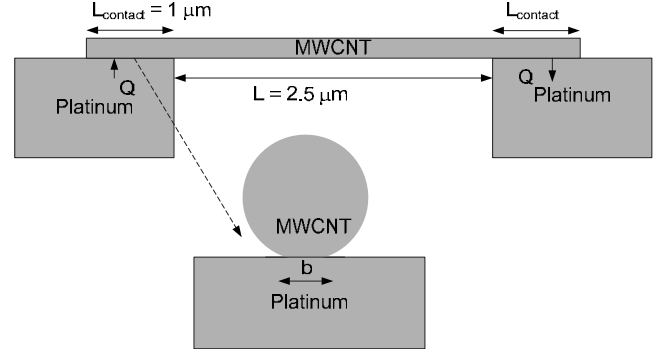


FIG. 5. Schematic of the device used by Kim *et al.* (Ref. 1) for the measurement of thermal conductivity of MWCNT. The heat enters the MWCNT through a very narrow constriction formed due to van der Waals forces between the MWCNT and the substrate.

listic resistances was a very good approximation for thin short wires and nanoconstrictions. In this approximation, the effective conductance is given by

$$G_{\text{eff}} = \frac{G_{B,a} G_{\text{diff},a}}{G_{B,a} + G_{\text{diff},a}} = \frac{k_a}{L}, \quad (10)$$

where  $G_{\text{diff}}$  is the diffusive conductance. Equation (10) is called the ballistic-diffusive approximation. It reduces to the correct limits in the case of fully ballistic transport or fully diffusive transport. In the intermediate regime, the error with exact solution of BTE is very small.<sup>51-53</sup> Using Eqs. (6), (8), and (10), it can be shown that Eq. (10) means that the effective mfp ( $l_{\text{eff}}$ ) is

$$l_{\text{eff}} = \frac{l_a l_{B,a}}{l_a + l_{B,a}} = \frac{2/\pi \times Ll_a}{2/\pi \times L + l_a}. \quad (11)$$

Equation (11) is nothing but the Matthiessen rule. Figure 4 shows the comparison between the experimental data and the conductivity given by Eq. (10). Figure 4 also shows that that thermal conductivity predicted by Eq. (10) is smaller than that predicted assuming completely ballistic or completely diffusive transport; however, it is still higher than the experimental data. In the next section, it is shown that if the thermal boundary resistance between the MWCNT and the measuring device is taken into account, then theoretical thermal conductivity assuming the mfp of bulk graphite is in good agreement with the experimental data.

## V. CALCULATION OF THERMAL BOUNDARY RESISTANCE

Figure 5 shows the schematic of the thermal measurement device used by Kim *et al.*<sup>1</sup> Figure 5 shows that heat is entering and leaving from the sides of the nanotube in contact with platinum. Due to van der Waals forces, the nanotube deforms and adheres to the platinum,<sup>54</sup> as shown in Fig. 5. The junction formed will be of the order of a few nanometers.<sup>54</sup> The junction acts as constriction to heat flow. At the contact between the MWCNT and platinum, there are two types of thermal resistances: (1) thermal boundary resistance due to mismatch in the acoustic properties of MWCNT

and platinum (Kapitza resistance) and (2) distortion of heat flux lines due to the constriction at the interface. The author has shown<sup>51</sup> that for nanosized constrictions, thermal resistance due to the mismatch in acoustic properties is much more dominant than that due to the constriction of the heat flux lines. Therefore, only thermal boundary resistance is included in the analysis.

In this section, thermal boundary resistance (also referred to as contact resistance) between graphite and an isotropic substrate is calculated.  $R_c$  is calculated for two orientations of graphite, as shown in Fig. 6. Horizontal orientation corresponds to the case shown for the measurement of thermal conductivity of MWCNT in Fig. 5. Vertical orientation is applicable to cases where MWCNTs are grown vertically on a substrate.<sup>7-9</sup> Vertically grown MWCNTs have been proposed as thermal interface materials.<sup>7-9</sup> Since graphite is anisotropic, i.e., velocity of phonons is different in different directions,  $R_c$  of graphite will be also different for horizontal and vertical orientations. The contact conductance ( $G_c$ ) for

the horizontal orientation, i.e., for the  $c$ -axis direction, can be written as

$$G_c = \frac{1}{2} \frac{1}{(2\pi)^3} \sum_3 \frac{d}{dT} \int_q \alpha_{1-2} \hbar \omega f |v_{g,z,1}| dq = \frac{1}{R_c}, \quad (12)$$

where  $\alpha_{1-2}$  is the transmissivity between material 1 (graphite) and material 2 (substrate). Writing  $dq = 2\pi q_a dq_a dq_z$ , Eq. (12) can be written as

$$G_c = \frac{1}{2} \frac{1}{(2\pi)^2} \sum_3 \frac{d}{dT} \int_0^{q_{a,\max}} \int_0^{q_{z,\max}} \alpha_{1-2} \hbar \omega f v_{g,z,1} q_a dq_a dq_z. \quad (13)$$

To calculate  $\alpha_{1-2}$ , the diffuse mismatch model (DMM) is used.<sup>55</sup> In DMM,  $\alpha_{1-2} = 1 - \alpha_{2-1}$ . Applying the law of detailed balance and assuming the gray medium approach of Chen *et al.*,<sup>56</sup>  $\alpha_{1-2}$  can be written as

$$\alpha_{1-2}(T) = \frac{\frac{1}{4} \sum_3 \int_0^{\omega_{\max}} \hbar \omega f v_{g,2} d\omega}{\frac{1}{2} \frac{1}{(2\pi)^2} \sum_3 \int_0^{q_{a,\max}} \int_0^{q_{z,\max}} \hbar \omega f v_{g,z,1} q_a dq_a dq_z + \frac{1}{4} \sum_3 \int_0^{\omega_{\max}} \hbar \omega f v_{g,2} d\omega}, \quad (14)$$

where  $v_{g,2}$  is the group velocity of phonons in material 2 (assumed isotropic). Similarly for the vertical case, contact conductance can be written as

$$G_{c,a} = 2 \frac{1}{(2\pi)^3} \sum_3 \frac{d}{dT} \int_0^{q_{a,\max}} \int_0^{q_{z,\max}} \hbar \omega \alpha_{1-2} f v_{g,a} q_a dq_a dq_z = \frac{1}{R_{c,a}}, \quad (15)$$

and

$$\alpha_{1-2,a}(T) = \frac{\frac{1}{4} \sum_3 \int_0^{\omega_{\max}} \hbar \omega f v_{g,2} d\omega}{2 \frac{1}{(2\pi)^3} \sum_3 \int_0^{q_{a,\max}} \int_0^{q_{z,\max}} \hbar \omega \alpha_{1-2} f v_{g,a} q_a dq_a dq_z + \frac{1}{4} \sum_3 \int_0^{\omega_{\max}} \hbar \omega f v_{g,2} d\omega}. \quad (16)$$

Note that the contact conductance given by Eqs. (13) and (15) is expressed on a per unit area basis ( $\text{W}/\text{m}^2 \text{K}$ ). Figure 7 shows the contact conductance for the basal plane direction and the  $c$ -axis direction between MWCNT (graphite) and platinum assuming the Debye model for platinum. Platinum is chosen because Kim *et al.*<sup>1</sup> used a platinum substrate. Figure 7 shows that the contact conductance in the basal plane is higher than the  $c$  direction due to the reduced effective velocity of phonons in the  $c$  direction, as compared to the basal plane. Figure 7 also shows that the anisotropy in the contact conductance decreases with decreasing temperature. The anisotropy in thermal conductivity of graphite shows a similar behavior both theoretically and experimentally.<sup>14,15</sup>

For the experimental structure of Kim *et al.*,<sup>1</sup> as shown in Fig. 5, the analysis of the contact resistance is complicated

because of the complexity of the heat flux lines near the contact. The heat enters in the direction of the  $c$  axis near the contact region, and then after some length, it flows in the  $a$ -axis direction. Due to this, the MWCNT in contact with the substrate acts as a fin.<sup>57</sup> Yu *et al.*<sup>57</sup> measured the thermal contact resistance and thermal conductivity of carbon nanofibers using the setup shown in Fig. 5. Based on the fin approach, they derived the apparent thermal contact resistance (in  $\text{W}/\text{K}$ ) as

$$R_c'' = \frac{2}{\sqrt{\frac{k_a \pi D^2}{4R_c'} \tanh\left(L_{\text{contact}} \sqrt{\frac{4}{k_a \pi D^2 R_c'}}\right)}}, \quad (17)$$

where  $R_c''$  is the apparent contact resistance,  $D$  the diameter of the MWCNT,  $L_{\text{contact}}$  the length of the MWCNT in contact

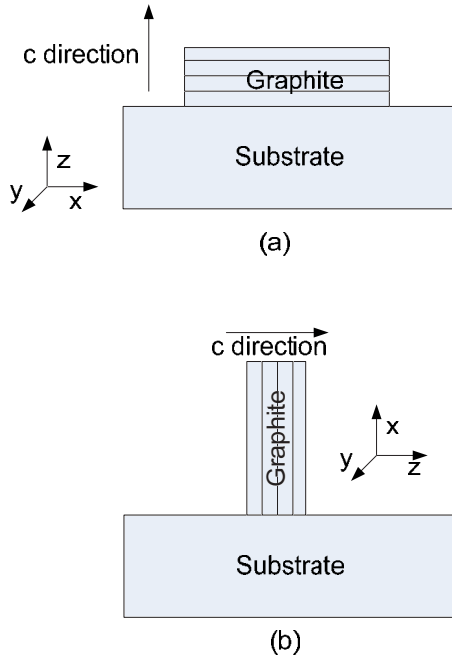


FIG. 6. (Color online) Schematic showing the different orientations of graphite (MWCNT) [(a) horizontal contact and (b) vertical contact] on a substrate for which thermal boundary resistance has been calculated.

with the substrate, and  $R'_c$  the contact resistance for unit length (in W m/K).  $R'_c$  is related to  $R_c$  by  $R'_c = R_c/b$ , where  $b$  is the contact width, as shown in Fig. 5. Note that Eq. (17) is strictly valid for fully diffusive transport, whereas the transport in the MWCNT used by Kim *et al.*<sup>1</sup> is ballistic-diffusive. If  $R_c$  is zero, then Eq. (17) shows that  $R'_c = 0$ . The total thermal resistance ( $R_{\text{tot}}$ ) for the geometry shown in Fig. 5 is given by

$$R_{\text{tot}} = R'_c + \frac{L}{k_a \times \pi/4 \times D^2}. \quad (18)$$

If the fin efficiency is not considered, then

$$R_{\text{tot}} = \frac{2R_c}{bL_{\text{contact}}} + \frac{L}{k_a \times \pi/4 \times D^2}. \quad (19)$$

In writing Eqs. (18) and (19), the inner diameter of MWCNT is assumed to be much smaller than the outer diameter.<sup>42</sup> Kim *et al.*<sup>1</sup> measured  $R_{\text{tot}}$  in their experiment. They assumed  $R_c = 0$  to derive the thermal conductivity. While comparing the data with theoretical calculations,  $R_c = 0$  was assumed in Fig. 4.  $R_c$  is calculated using Eq. (13) and  $k_a$  is obtained using both Eqs. (18) and (19) to understand the impact of the fin effect.

Contact width ( $b$ ) is needed in Eqs. (18) and (19). Contact width of a cylinder in contact with a planar substrate due to van der Waals forces was calculated by Sari *et al.*<sup>58</sup> and Baney and Hui.<sup>59</sup> Using their relations

$$b = 4 \left( \frac{D^2 w}{4\pi E} \right)^{1/3} \lambda \sqrt{m^2 - 1}, \quad (20)$$

where  $w$  is the adhesion energy per unit area,  $E^{-1} = (1 - \nu_1^2)/E_1 + (1 - \nu_2^2)/E_2$ , where  $E$  is the Young modulus and  $\nu$  is the Poisson ratio. For graphite, the Young modulus and the Poisson ratio in the  $c$ -axis direction are used for calculations.  $\lambda$  in Eq. (20) is given by

$$\lambda = \frac{4\sigma_0}{(2\pi^2 E^2 w/D)^{1/3}}, \quad (21)$$

where  $\sigma_0$  is the theoretical strength of the joint. If the surface force for the adhesion is modeled assuming the Lennard-Jones model, then  $w = A/(16\pi z_0^2)$  (Ref. 60) and  $\sigma_0 = w/(0.97z_0)$ ,<sup>58</sup> where  $A$  is the Hamaker constant and  $z_0$  is the equilibrium separation between the MWCNT and the platinum.  $z_0$  is assumed to be the same as the interlayer separation in graphite (0.335 nm). Akita *et al.*<sup>61</sup> measured the Hamaker constant of MWCNTs in contact with metals where the contact was along the length of MWCNTs. The Hamaker constant was found to be  $60 \times 10^{-20}$  J. This value of  $A$  is used in calculating  $w$ .  $m$  in Eq. (20) is given as<sup>58</sup>

$$\begin{aligned} 1/2\lambda^3 \{ (m^2 - 1)[m\sqrt{m^2 - 1} - \ln(m + \sqrt{m^2 - 1})] \\ + \sqrt{m^2 - 1}[\sqrt{m^2 - 1}\ln(m + \sqrt{m^2 - 1}) - m \ln m] \} = 1. \end{aligned} \quad (22)$$

Various properties needed to calculate the contact width are given in Table I. Note that for the  $c$  axis,  $E \approx c_{33}$ .<sup>22</sup> Assuming the MWCNT diameter of 14 nm, the contact width from Eq. (20) is 1.25 nm.

Figure 8 shows the comparison between the thermal conductivity obtained from the experimental data using Eqs. (18) and (19) and those from the theoretical calculations using Eq. (10). Thermal conductivity by considering the fin

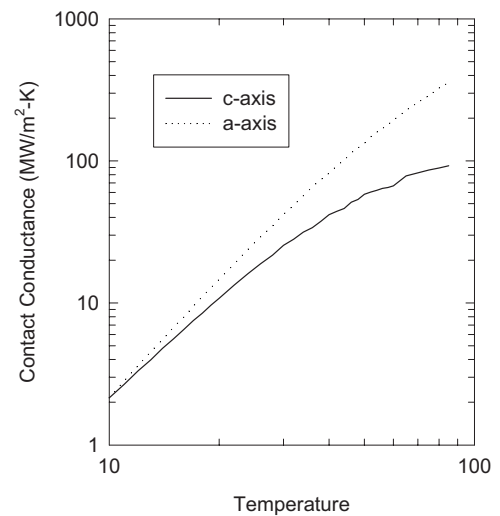


FIG. 7. Thermal contact conductance between graphite and platinum for the basal plane (vertical contact) and  $c$ -axis (horizontal contact) directions as a function of temperature. Similar to the thermal conductivity, the anisotropy in contact conductance decreases with decreasing temperature.

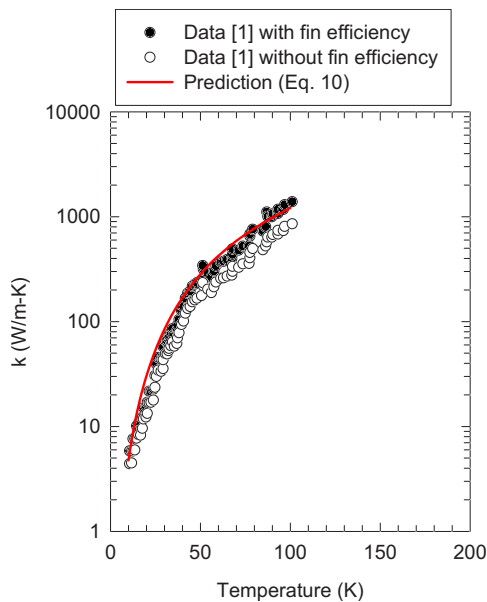


FIG. 8. (Color online) Comparison between the predicted and experimental thermal conductivities by including the thermal boundary resistance and using the recommended properties of graphite (Table I).

effect is slightly larger than the thermal conductivity without the fin effect. Figure 8 shows that theoretical calculations are in excellent agreement with the experimental data. This shows that using the properties of graphite, thermal conductivity of MWCNT can be well described. Thermal conductivity is also calculated by considering smaller values of  $c_{44}$  (0.7 GPa) and  $c_{33}$  (20 GPa) to understand the effects of reduction in interlayer coupling as compared to graphite. Figure 9 shows that although the predicted thermal conductivity is slightly higher than the data, however, it is still in good agreement with the data.  $k$ ,  $R_c$ , and  $b$  are calculated assuming the modified properties for Fig. 9.

It is to be noted that the thermal conductivity measured by Fujii *et al.*<sup>2</sup> is smaller than the thermal conductivity measured by Kim *et al.*<sup>1</sup> for  $T < 200$  K, as shown in Fig. 1. There are two potential reasons for that. The suspended length of the MWCNT in their study was  $1.89 \mu\text{m}$  as compared to  $2.5 \mu\text{m}$  in the study by Kim *et al.*<sup>1</sup> This reduces the effective mean free path [Eq. (11)]. The second reason could be the difference in contact resistance in the two measurements. No details regarding the contact region were provided by Fujii *et al.*<sup>2</sup>

## VI. THERMAL CONDUCTIVITY OF BUNDLES

A significant amount of work has been done on the thermal transport and the specific heat of SWCNT bundles (also called ropes).<sup>48,62–65</sup> To the best of our knowledge, thermal conductivity of MWCNT bundles has only been measured by Kim *et al.*<sup>1</sup> Phonon dispersion in SWCNT bundles can be different from phonon dispersion in isolated SWCNTs.<sup>36,48</sup> Modeling of the specific heat of SWCNT bundles using modified phonon dispersion has yielded mixed results, as compared to experimental data.<sup>48</sup> For MWCNT bundles con-

sidered in this study, it is expected that phonon dispersion of individual MWCNTs in the bundle should not change, as compared to an isolated single MWCNT because  $q_d(r_2 - r_1) \approx q_d r_2 > 1$  for the MWCNT used by Kim *et al.*,<sup>1</sup> as discussed before. This means that the nanotube boundary should not play a significant role in phonon dispersion. It is to be noted that for sufficiently lower temperatures ( $q_d r_2 < 1$ ), it is possible that coupling between the nanotubes can change the phonon dispersion. This can lead to a change in the specific heat and the thermal conductivity of bundles, as compared to the individual MWCNTs. For SWCNTs at low temperatures, typically  $q_d r_2 < 1$  because of the small size of the SWCNTs ( $r_2 < 1$  nm investigated in the literature<sup>48,62–65</sup>). Walls of SWCNTs are also only one atomic layer thick. Due to these reasons, phonon dispersion of SWCNT bundles can be significantly different from individual SWCNTs because the nanotube boundary will play a significant role particularly if tube-to-tube interactions are strong. Based on these discussions, phonon dispersion in MWCNT in the bundle can be safely assumed to be the same as the phonon dispersion in isolated MWCNT.

The diameters of the two bundles measured by Kim *et al.*<sup>1</sup> were 80 and 200 nm. Exact geometrical configuration of the bundles was not known in their study. Assuming the bundles as a cylindrical object, they obtained the thermal conductivity of the bundles. Thermal conductivity of the bundles was much smaller than the thermal conductivity of single MWCNT. Thermal conductivity of the 200 nm bundle was smaller than the thermal conductivity of the 80 nm bundle. Bundles of graphite fibers, on the other hand, have the same thermal conductivity as a single graphite fiber.<sup>13</sup>

To model the thermal conductivity of the bundles, the bundles are assumed to be of cylindrical shape. Based on this

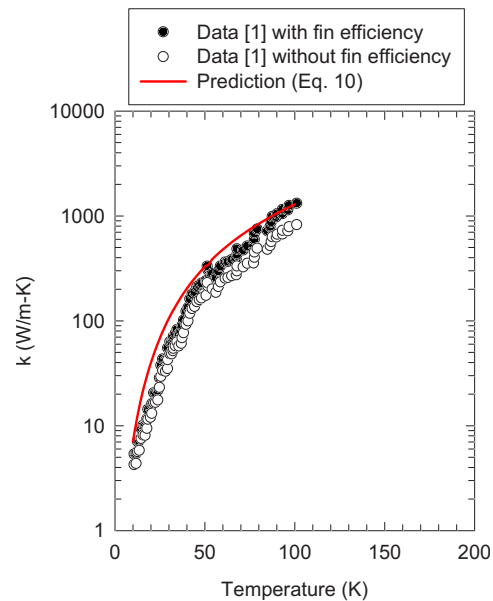


FIG. 9. (Color online) Comparison between the predicted and experimental thermal conductivities by including the thermal boundary resistance and assuming  $c_{44}=0.7$  GPa and  $c_{33}=20$  GPa. Reduced values of  $c_{44}$  and  $c_{33}$  are used to reflect reduction in inter-tube coupling in MWCNTs, as compared to graphite (see text for details).

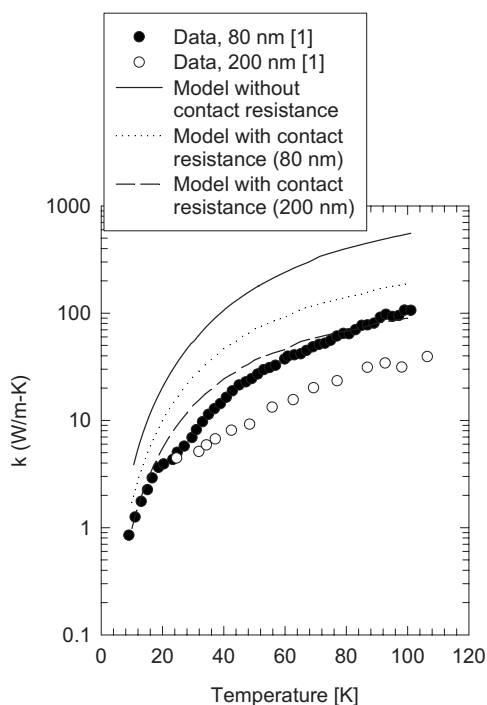


FIG. 10. Comparison between the prediction and data for bundles assuming the bundles to be solid cylinders. The contact width is calculated using Eq. (20). Trends obtained from the prediction by including the contact resistance are consistent with the experimental trends, i.e., thermal conductivity of single MWCNT (not shown here) is higher than the thermal conductivity of the 80 nm bundle which in turn is higher than the thermal conductivity of the 200 nm bundle.

assumption, the contact widths for the 80 nm bundle from Eq. (20) are 4.7 and 9.4 nm for the 200 nm bundle. Figure 10 shows the comparison between the model and the experiment. Theoretical calculations including the contact resistance show the same trend as the experimental data, i.e., thermal conductivity of the single MWCNT (not shown in Fig. 10) is higher than the thermal conductivity of the 80 nm bundle which is higher than the thermal conductivity of the 200 nm bundle. For larger bundles, the impact of contact resistance is more because the bulk thermal resistance of the larger bundles is smaller than the bulk resistance of the smaller bundles or single MWCNT. The model predictions do not match with the data very well because of simplifying assumptions such as modeling the bundles as solid cylinders. It is quite possible that only one or two nanotubes are touching the substrate in the bundles. If the effective contact width is assumed to be 2 nm for the 80 nm bundle and 3 nm for the 200 nm bundle, then the match is better with the experimental data, as shown in Fig. 11. Irrespective of whether the theoretical calculations match with the data or not, it is safe to say that contact resistance could play a significant role in the data trend obtained for single MWCNT and bundles of different diameters for the experimental setup shown in Fig. 5.

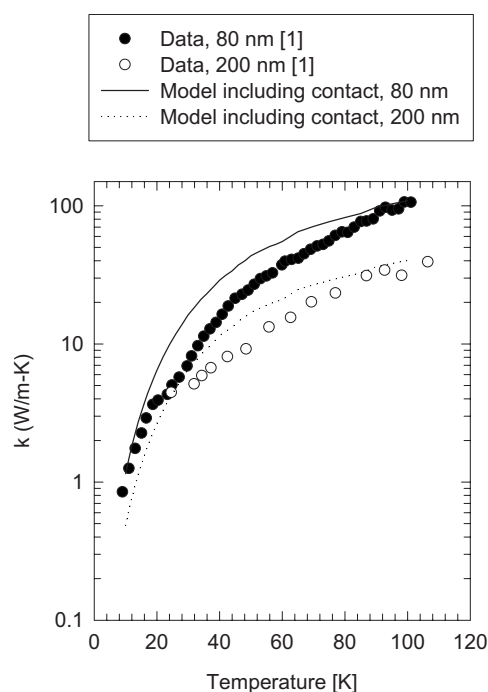


FIG. 11. Comparison between the prediction and data for bundles assuming that only a few nanotubes in the bundles touch the substrate. Effective contact width of the 80 nm bundle is assumed to be 2 nm and for the 200 nm bundle is assumed to be 3 nm.

## VII. CONCLUSIONS

Thermal conductivity and thermal boundary resistance (contact resistance) of MWCNTs were calculated in the temperature range of 10–100 K. Results show that the thermal behavior of MWCNTs is similar to graphite and the thermal conductivity of MWCNTs can be modeled assuming the properties and parameters of graphite, although it is possible that the interlayer coupling in MWCNTs might be slightly different than it is in graphite. It was also shown that phonon confinement effects in MWCNTs are important only at very low temperatures. Contact resistance between MWCNTs (graphite) and bulk 3D isotropic substrates was modeled for both vertical and horizontal contacts. Contact conductance in the vertical direction is higher than the conductance in the horizontal direction. The predicted thermal conductivity is in good agreement with experimental data if contact resistance between the MWCNT and the measuring device is taken into consideration. It was also shown that contact resistance plays a significant role in the measured value of thermal conductivity of MWCNT bundles.

## ACKNOWLEDGMENTS

The author thanks Philip Kim for sending the raw data of the experimental measurements and Li Shi for very helpful discussions.

- \*Also at Department of Mechanical and Aerospace Engineering, Arizona State University; ravi.s.prasher@intel.com
- <sup>1</sup>P. Kim, L. Shi, A. Majumdar, and P. L. McEuen, *Phys. Rev. Lett.* **87**, 215502 (2001).
  - <sup>2</sup>M. Fujii, X. Zhang, H. Xie, K. Takahashi, T. Ikuta, H. Abe, and T. Shimizu, *Phys. Rev. Lett.* **95**, 065502 (2005).
  - <sup>3</sup>H.-Y. Chiu, V. V. Deshpande, H. W. Postma, C. N. Lau, C. Miko, L. Forro, and M. Bockrath, *Phys. Rev. Lett.* **95**, 226101 (2005).
  - <sup>4</sup>E. Pop, D. Mann, J. Cao, Q. Wang, K. Goodson, and H. Dai, *Phys. Rev. Lett.* **95**, 155505 (2005).
  - <sup>5</sup>N. Mingo and D. A. Broido, *Phys. Rev. Lett.* **95**, 096105 (2005).
  - <sup>6</sup>H. Zhong and J. R. Lukes, *Phys. Rev. B* **74**, 125403 (2006).
  - <sup>7</sup>J. Xu and T. S. Fisher, *IEEE Trans. Compon. Packag. Technol.* **29**, 261 (2006).
  - <sup>8</sup>X. J. Hu, A. Padilla, J. Xu, T. S. Fisher, and K. E. Goodson, *J. Heat Transfer* **128**, 1109 (2006).
  - <sup>9</sup>T. Tong, T. Zhao, L. Delzeit, A. Kashani, M. Meyyappan, and A. Majumdar, *IEEE Trans. Compon. Packag. Technol.* **30**, 92 (2007).
  - <sup>10</sup>R. Sivakumar, S. Guo, T. Nishimura, and Y. Kagawa, *Scr. Mater.* **56**, 265 (2007).
  - <sup>11</sup>R. S. Prasher, *Proc. IEEE* **94**, 1571 (2006).
  - <sup>12</sup>Y. Yang, E. Grulke, Z. G. Zhang, and G. Wu, *J. Appl. Phys.* **99**, 114307 (2006).
  - <sup>13</sup>L. Piraux, B. Nysten, A. Haquenne, J.-P. Issi, M. S. Dresselhaus, and M. Endo, *Solid State Commun.* **50**, 697 (1984).
  - <sup>14</sup>C. N. Hooker, A. R. Ubbelohde, and D. A. Young, *Proc. R. Soc. London, Ser. A* **284**, 1396 (1965).
  - <sup>15</sup>G. A. Slack, *Phys. Rev.* **127**, 694 (1962).
  - <sup>16</sup>R. Taylor, *Philos. Mag.* **13**, 157 (1966).
  - <sup>17</sup>M. R. Null, W. W. Lozier, and A. W. Moore, *Carbon* **11**, 81 (1973).
  - <sup>18</sup>J. Heremans, and C. P. Beetz, Jr., *Phys. Rev. B* **32**, 1981 (1985).
  - <sup>19</sup>P. G. Klemens and D. F. Pedraza, *Carbon* **32**, 735 (1994).
  - <sup>20</sup>E. Pop, D. Mann, Q. Wang, K. Goodson, and H. Dai, *Nano Lett.* **6**, 96 (2006).
  - <sup>21</sup>K. Komatsu, *J. Phys. Soc. Jpn.* **10**, 346 (1955).
  - <sup>22</sup>B. T. Kelly, *Physics of Graphite* (Applied Science, London, 1981).
  - <sup>23</sup>B. T. Kelly, *Carbon* **5**, 247 (1967).
  - <sup>24</sup>W. N. Reynolds, *Physics Properties of Graphite* (Elsevier, Amsterdam, 1968).
  - <sup>25</sup>L. Shen and J. Li, *Phys. Rev. B* **71**, 035412 (2005).
  - <sup>26</sup>K. Komatsu and T. Nagamiya, *J. Phys. Soc. Jpn.* **6**, 438 (1951).
  - <sup>27</sup>M. S. Dresselhaus, G. Dresselhaus, and P. Avouris, *Carbon Nanotubes: Synthesis, Structure, Properties and Applications* (Springer, New York, 2001).
  - <sup>28</sup>C. Q. Chen, Y. Shi, Y. S. Zhang, J. Zhu, and Y. J. Yan, *Phys. Rev. Lett.* **96**, 075505 (2006).
  - <sup>29</sup>M. X. Gu, T. C. Yeung, C. M. Tan, and V. Nosik, *J. Appl. Phys.* **100**, 094304 (2006).
  - <sup>30</sup>L. G. C. Rego and G. Kirczenow, *Phys. Rev. Lett.* **81**, 232 (1998).
  - <sup>31</sup>N. Nishiguchi, Y. Ando, and M. N. Wybourne, *J. Phys.: Condens. Matter* **9**, 5751 (1997).
  - <sup>32</sup>K. F. Graff, *Wave Motion in Elastic Solids* (Dover, New York, 1991).
  - <sup>33</sup>G. D. Mahan, *Phys. Rev. B* **65**, 235402 (2002).
  - <sup>34</sup>G. D. Mahan and G. S. Jeon, *Phys. Rev. B* **70**, 075405 (2004).
  - <sup>35</sup>V. N. Popov, V. E. Van Doren, and M. Balkanski, *Phys. Rev. B* **61**, 3078 (2000).
  - <sup>36</sup>M. S. Dresselhaus and P. C. Eklund, *Adv. Phys.* **49**, 705 (2000).
  - <sup>37</sup>T. Klitsner and R. O. Pohl, *Phys. Rev. B* **36**, 6551 (1987).
  - <sup>38</sup>J. M. Ziman, *Electrons and Phonons* (Oxford University Press, New York, 1960).
  - <sup>39</sup>O. Bourgeois, T. Fournier, and J. Chaussy, *J. Appl. Phys.* **101**, 016104 (2007).
  - <sup>40</sup>K. Schwab, E. A. Henriksen, J. M. Worlock, and M. L. Roukes, *Nature (London)* **404**, 974 (2000).
  - <sup>41</sup>R. Prasher, *Phys. Rev. B* **74**, 165413 (2006).
  - <sup>42</sup>Li Shi (private communication).
  - <sup>43</sup>V. N. Popov, *Phys. Rev. B* **66**, 153408 (2002).
  - <sup>44</sup>W. Guo, Y. Guo, H. Gao, Q. Zheng, and W. Zhong, *Phys. Rev. Lett.* **91**, 125501 (2003).
  - <sup>45</sup>C. A. Klein and M. G. Holland, *Phys. Rev.* **136**, A575 (1964).
  - <sup>46</sup>C. Q. Ru, *Phys. Rev. B* **62**, 16962 (2000).
  - <sup>47</sup>I. Palaci, S. Fedrigo, H. Brune, C. Klinke, M. Chen, and E. Riedo, *Phys. Rev. Lett.* **94**, 175502 (2005).
  - <sup>48</sup>A. Mizel, L. X. Benedict, M. L. Cohen, S. G. Louie, A. Zettl, N. K. Budraa, and W. P. Beyermann, *Phys. Rev. B* **60**, 3264 (1999).
  - <sup>49</sup>C. Masarapu, L. L. Henry, and B. Wei, *Nanotechnology* **16**, 1490 (2005).
  - <sup>50</sup>P. Carruthers, *Rev. Mod. Phys.* **33**, 92 (1961).
  - <sup>51</sup>R. Prasher, *J. Appl. Phys.* **100**, 064302 (2006); R. Prasher and R. S. Prasher, *Nano Lett.* **5**, 2155 (2005); R. S. Prasher and P. E. Phelan, *J. Appl. Phys.* **100**, 063538 (2006).
  - <sup>52</sup>B. Nikolić and P. B. Allen, *Phys. Rev. B* **60**, 3963 (1999).
  - <sup>53</sup>M. J. M. de Jong, *Phys. Rev. B* **49**, 7778 (1994).
  - <sup>54</sup>H. Maune, H.-Y. Chiu, and M. Bockrath, *Appl. Phys. Lett.* **89**, 013109 (2006).
  - <sup>55</sup>E. T. Swartz and R. O. Pohl, *Rev. Mod. Phys.* **61**, 605 (1989).
  - <sup>56</sup>G. Chen, *Phys. Rev. B* **57**, 14958 (1998); R. Yang and G. Chen, *ibid.* **69**, 195316 (2004).
  - <sup>57</sup>C. Yu, S. Saha, J. Zhou, L. Shi, A. M. Cassel, B. A. Cruden, Q. Ngo, and J. Li, *J. Heat Transfer* **128**, 234 (2006).
  - <sup>58</sup>O. T. Sari, G. G. Adams, and S. Muftu, *J. Appl. Mech.* **72**, 633 (2005).
  - <sup>59</sup>J. M. Baney and C.-Y. Hui, *J. Adhes. Sci. Technol.* **11**, 393 (1997).
  - <sup>60</sup>P. Attard and J. L. Parker, *Phys. Rev. A* **46**, 7959 (1992).
  - <sup>61</sup>S. Akita, H. Mishijima, and Y. Nakayama, *J. Phys. D* **33**, 2673 (2000).
  - <sup>62</sup>J. Hone, B. Batlogg, Z. Benes, A. T. Johnson, and J. E. Fischer, *Science* **289**, 1730 (2000).
  - <sup>63</sup>J. Hone, M. C. Llaguno, M. J. Biercuk, B. Batlogg, Z. Benes, A. T. Johnson, and J. E. Fischer, *Appl. Phys. A: Mater. Sci. Process.* **74**, 339 (2002).
  - <sup>64</sup>J. Hone, M. Whitney, C. Piskoti, and A. Zettl, *Phys. Rev. B* **59**, R2514 (1999).
  - <sup>65</sup>L. Shi, D. Li, C. Yu, W. Jang, D. Kim, Z. Yao, P. Kim, and A. Majumdar, *J. Heat Transfer* **125**, 881 (2003).